A. F. García-Fernández, O. A. Yeste-Ojeda and J. Grajal, "Facet Model of Moving Targets for ISAR Imaging and Radar Back-Scattering Simulation," in IEEE Transactions on Aerospace and Electronic Systems, vol. 46, no. 3, pp. 1455-1467, July 2010, doi: 10.1109/TAES.2010.5545200.

Facet model of moving targets for ISAR imaging and radar back-scattering simulation

Ángel F. García-Fernández, Omar A. Yeste-Ojeda *Member IEEE*, Jesús Grajal

Abstract

A facet model of targets is proposed to simulate ISAR images and radar back-scattering of moving targets with rigid and nonrigid motions. Targets are composed of solid objects which are modeled by triangular facets. It is shown that a facet can be treated as an equivalent point-scatterer whose radar cross section and position depend on the shape of the triangle, the frequency and the angle of incidence. A shadowing algorithm is also developed to detect the facets which actually have influence on the signal received by the radar. Besides, a facet division algorithm is implemented to improve the result of the shadowing algorithm and to have at least one facet per resolution cell. Finally, we apply our simulator to obtain the ISAR images of a ship and a helicopter and to calculate the micro-Doppler signature of a human.

Keywords: Delaunay triangulation, facet, human gait, ISAR, micro-Doppler.

I. Introduction

Inverse synthetic aperture radar (ISAR) imaging maps the reflectivity function of a target onto a range and Doppler plane [1]. This projection is performed by coherently processing the echoes from a moving target. The ISAR images can provide information for non-cooperative target recognition [2], [3]. Nevertheless, this information can be useless if the target motion produces blurred images. Motion compensation algorithms [4]–[8] or time-frequency techniques [9]–[15] are useful techniques to solve this problem.

It is very complicated to carry out controlled experiments to generate ISAR images so the development of a software tool is needed. There have been two main approaches to model targets, the point-scatterer model and the electromagnetic model. The point-scatterer model is the simplest one but the ISAR images obtained are not realistic enough according to the measured data [1], [16], [17]. The point-scatterer model can be established from electromagnetic theory. This is done through the high-frequency approximation to Maxwell's equations, or ray optics. It was shown that the electromagnetic scattering from a complex target can be described by a set of localized ray phenomena [16]. The model based on the use of computational electromagnetic modeling tools [18], [19] provides the most realistic ISAR images but it requires high computational burden.

We propose a model, which was briefly introduced in [20], based on perfectly conducting triangular facets. Triangular shapes have been chosen on account of their versatility to approximate complex objects. This model has the properties of requiring less computational burden than the electromagnetic model, providing more realistic images than the point-scatterer model and being able to deal with moving targets that have nonrigid motions. However, our model does not take into account multiple scattering. Other facet models proposed up to now to calculate radar cross sections [19], [21], [22] or ISAR images [23], [24] deal directly with electromagnetic fields or with the physical optics approximation. These models have problems when the aim is to calculate the returned signal from a target which has a nonrigid body motion. On the other hand, our model introduces a compact equation to calculate the received signal in which each facet is regarded as an equivalent point-scatterer with a certain radar cross section and position. In addition, it is capable of calculating the returned signal from a moving target.

In Section II, the target and the received signal models are presented. It is also shown that a facet can be represented as an equivalent point-scatterer whose radar cross section and localization depend on the shape of the facet, the angle of incidence and the carrier frequency. A shadowing algorithm is also developed to find the visible facets. In Section III, some practical issues such as the facet division algorithm, the noise level consideration and the validation of the model are explained. The application of the facet model to ISAR imaging of moving targets is addressed in Section IV. In Section V, we show how to use our model to calculate the radar back-scattering from a human. Finally, conclusions are drawn in Section VI.

II. Target model and received signal

In our model, each facet is regarded as a point-scatterer whose radar cross section and position depend on the shape of the facet, the angle of incidence and the frequency. Thus, the problem is to determine the radar cross section and the position of the equivalent point-scatterer.

The radar is located at the origin of the coordinate system $OUVW$. The target is composed of a set of solid objects modeled by triangular facets. Each facet consists of a triangle and a unitary vector $\hat{n}$ which is orthogonal to the triangle[1]. This vector

The authors are with the Grupo de Microondas y Radar, Departamento de Señales, Sistemas y Radiocomunicaciones, ETSI de Telecomunicación, Universidad Politécnica Madrid, Ciudad Universitaria s/n, 28040 Madrid, Spain. email: agarcia@gmr.ssr.upm.es, omar@gmr.ssr.upm.es, jesus@gmr.ssr.upm.es

[1]The notation $\hat{a}$ indicates that vector $\hat{a}$ is a unitary vector.

indicates the active face of the facet. The active face is the external face of the facet in relation to the solid object which the facet belongs to. The use of the active face is useful to reduce the computational load of the shadowing algorithm, as it is shown in subsection II-C. The radar is assumed to transmit a rectangular pulsed waveform with a carrier frequency f_c, with a pulse repetition interval T_{PRI}. If $t \in [0,\, T_{PRI}]$, the returned baseband signal from a target is:

$$s(t) = \sum_{i=1}^{M} \psi_i \cdot \sqrt{\sigma_i}\, e^{-j\frac{2\pi f_c}{c}2R_i} rect\left(t - \frac{2R_i}{c}, T\right) + n\,(t) \tag{1}$$

where the rectangular pulse is defined as

$$rect(t,\, T) = \begin{cases} 1 & t \in [0,\, T] \\ 0 & otherwise \end{cases} \tag{2}$$

where T is the duration of the rectangular pulse, c is the velocity of the wave propagation, M is the number of facets of the target, σ_i is the radar cross section of the facet i, R_i is the range of the facet i measured from the origin of the coordinate system $OUVW$, ψ_i is a function whose value is one if the facet i is visible from the radar and zero otherwise and $n\,(t)$ represents undesired signals such as receiver's noise or clutter. The parameters σ_i, R_i and ψ_i are assumed to be constant during the pulse repetition interval. The aim of this Section is to compute $s(t)$, so the parameters σ_i, R_i and ψ_i are analyzed in subsections II-A, II-B and II-C, respectively. On the other hand, the noise $n\,(t)$ is analyzed in Section III.

A. Radar cross section

[Figure 1 about here.]

The radar cross section of a perfectly conducting surface S situated on the plane O_BXY_{SR} when the plane of incidence is the XZ_{SR} plane, as shown in Fig. 1, assuming plane wave conditions and the fact that the smallest dimension of the surface is several wavelengths long, is given by the equation [25]:

$$\sigma_S = \frac{4\pi}{\lambda^2}\cos^2\theta \left| \int_S e^{-j2kx_{SR}\sin\theta} dS \right|^2 \tag{3}$$

where λ is the wavelength of the transmitted signal, θ is the angle between the incident wave and the O_BZ_{SR} axis and $k = 2\pi/\lambda$ is the wave number.

In order to apply equation (3) to a surface placed on any plane of the space, it is needed to use the coordinate system O_BXYZ_{SR}, as illustrated in Fig. 2, so that the surface S is situated on the plane O_BXY_{SR} and the plane of incidence is XZ_{SR}. In our facet model, S is a triangle, O_B is the barycenter of the triangle (another point of the plane of the triangle can be taken as long as plane wave conditions can be assumed) and the unitary vectors that form the base $\hat{x}_{SR}$, $\hat{y}_{SR}$ and $\hat{z}_{SR}$ are defined by the following equations when $\theta \neq 0$:

$$\hat{z}_{SR} = \hat{n} \tag{4}$$

$$\hat{y}_{SR} = \frac{\hat{z}_{SR} \times \overrightarrow{O_BO}}{\left|\hat{z}_{SR} \times \overrightarrow{O_BO}\right|} \tag{5}$$

$$\hat{x}_{SR} = \hat{y}_{SR} \times \hat{z}_{SR} \tag{6}$$

where $\hat{n}$ is the unitary vector that is orthogonal to the triangle and indicates the active face of the facet.

It must be noted that when the incident wave is orthogonal to the triangle, $\theta = 0$, the vector $\hat{y}_{SR}$ cannot be calculated with equation (5) because vectors $\hat{z}_{SR}$ and $\overrightarrow{O_BO}$ are proportional and, thus, their cross product is the null vector. Nevertheless, if $\theta = 0$ the radar cross section is, using equation (3):

$$\sigma_S = \frac{4\pi}{\lambda^2}\,(A_S)^2 \tag{7}$$

where A_S is the area of the triangle, and, therefore, the coordinate system O_BXYZ_{SR} does not have to be defined to calculate the radar cross section.

[Figure 2 about here.]

B. Phase center of a facet

The next step is to calculate the position of the corresponding point-scatterer of the facet to determine the distance R between the facet and the radar. The position of the corresponding point-scatterer is obtained by imposing that when a plane surface S, placed in only one resolution cell, is divided into N surfaces S_1, S_2, ..., S_N, the returned signal from S must be equal to the sum of the returned signals from S_1, S_2, ...,S_N. First, it is needed to define the parameter I_S and substitute it into (3):

$$I_S \triangleq \int_S e^{j2kx_{SR}\sin\theta} dS \tag{8}$$

$$\sigma_S = \frac{4\pi}{\lambda^2}\cos^2\theta\,|I_S|^2 \tag{9}$$

Applying the additive property of integrals to (8):

$$I_S = \sum_{i=1}^{N}\int_{S_i} e^{j2kx_{SR}\sin\theta} dS_i = \sum_{i=1}^{N} I_{S_i} \tag{10}$$

The equation (10) can be expressed as:

$$|I_S|\, e^{j\angle I_S} = \sum_{i=1}^{N} |I_{S_i}|\, e^{j\angle I_{S_i}} \tag{11}$$

Due to the fact that the returned signal from S must be equal to the sum of the returned signals from S_1, S_2, ...,S_N:

$$s_S = \sum_{i=1}^{N} s_{S_i} \tag{12}$$

where the time dependence has been removed to use a less cumbersome notation, and s_{S_i} is the returned signal from surface S_i. It follows from (1) that:

$$\sqrt{\frac{4\pi}{\lambda^2}\cos^2\theta}\,|I_S|\, e^{-j2kR_S} = \sum_{i=1}^{N}\sqrt{\frac{4\pi}{\lambda^2}\cos^2\theta}\,|I_{S_i}|\, e^{-j2kR_{S_i}} \tag{13}$$

where a plane wave has been assumed so the angle of incidence θ is the same for all the surfaces. Simplifying (13):

$$|I_S|\, e^{-j2kR_S} = \sum_{i=1}^{N} |I_{S_i}|\, e^{-j2kR_{S_i}} \tag{14}$$

According to the definition of the coordinate system O_BXYZ_{SR}, the plane of incidence is XZ_{SR}, see Fig. 2. Then, the effect of the y_{SR} coordinate of a point-scatterer, located on S, on the phase of the received signal is negligible assuming plane wave conditions. Therefore, we situate the corresponding point-scatterer, X_i, on the O_BX_{SR} axis and the distance from the corresponding point-scatterer to the radar R_{S_i} can be expressed as:

$$R_{S_i} = \left|\overrightarrow{X_iO}\right| = \left|\overrightarrow{O_BO} - \overrightarrow{O_BX_i}\right| \tag{15}$$

where

$$\overrightarrow{O_BO} = (R_0\sin\theta,\, 0,\, R_0\cos\theta) \tag{16}$$

$$\overrightarrow{O_BX_i} = (x_{S_i},\, 0,\, 0) \tag{17}$$

In equations (16) and (17), the coordinates of the vectors are given in the coordinate system O_BXYZ_{SR}, x_{S_i} is the X_{SR} coordinate in the coordinate system O_BXYZ_{SR} that determines the position of the corresponding point-scatterer, X_i, and R_0 is the distance between the position of the radar O and O_B.

Substituting (16) and (17) in (15) and operating:

$$R_{S_i} = \sqrt{(R_0\sin\theta - x_{S_i})^2 + (R_0\cos\theta)^2} =$$

$$= \sqrt{(R_0)^2 + (x_{S_i})^2 - 2x_{S_i}R_0\sin\theta} =$$

$$= R_0\sqrt{1+\left(\frac{x_{S_i}}{R_0}\right)^2 - 2\frac{x_{S_i}}{R_0}\sin\theta} \tag{18}$$

If we call $p = \frac{x_{S_i}}{R_0}$ and we assume that $R_0 \gg x_{S_i}$, then $p \ll 1$ and R_{S_i} can be approximated by a first order Taylor polynomial. We use the notation $R_{S_i} = R_{S_i}(p)$ to stress that R_{S_i} is a function of p, therefore

$$R_{S_i}(p) \approx R_{S_i}(0) + p \cdot \frac{dR_{S_i}(0)}{dp} \tag{19}$$

Substituting (18) in equation (19) and operating, the distance from the radar to the equivalent point-scatterer is:

$$R_{S_i} \approx R_0 - x_{S_i}\sin\theta \tag{20}$$

Substituting (20) into (14):

$$|I_S|\, e^{-j2k(R_0 - x_S\sin\theta)} = \sum_{i=1}^{N} |I_{S_i}|\, e^{-j2k\left(R_0 - x_{S_i}\sin\theta\right)} \tag{21}$$

In view of (11), a solution for (21) when $\theta \neq 0$ is:

$$x_{S_i} = \frac{\angle I_{S_i}}{2k\sin\theta} \tag{22}$$

When $\theta \to 0$ in equation (22), the phase center tends to be the barycenter of the triangle (proof is given in the Appendix), therefore, when $\theta = 0$, X_i is located on O_B so that there is not a discontinuity, i. e., $x_{S_i} = 0$.

The point X_i, whose coordinates are $(x_{S_i}, 0, 0)$ in the coordinate system O_BXYZ_{SR}, is named the *phase center* of the facet i. The name *phase center* was given due to the fact that it was defined to determine the phase of the returned signal, i. e., the location of the equivalent point-scatterer, so that the returned signal from a surface is the same no matter what division we apply to the area. Placing the equivalent point-scatterer in the phase center, equation (12) holds and R_i is calculated. Thus, the range R_i of the facet i is calculated as the distance between its phase center and the radar.

The phase center is defined only by the coordinate x_{SR} since the coordinate z_{SR} of S is zero by definition and the effect of the coordinate y_{SR} on the phase of the received signal is negligible assuming plane wave conditions. Its position depends on the carrier frequency, the angle of incidence, the shape and the area of the facet.

C. Hidden facets

The next step to calculate equation (1) is to determine ψ_i. It is assumed that a facet is hidden if its barycenter is hidden by another facet. First of all, the mathematical conditions that must be satisfied when an arbitrary point P is hidden by the facet i are analyzed. The vectors $\vec{v}_{i1}$, $\vec{v}_{i2}$ and $\vec{v}_{i3}$ go from the origin of the coordinate system $OUVW$ to every vertex of the facet i, as shown in Fig. 3. Two sets of points are considered, Λ and Λ_{hidden}. The set Λ are the points which belong to the infinite tetrahedron whose apex is the origin of the coordinate system $OUVW$ and whose sides are determined by the vectors $\vec{v}_{i1}$, $\vec{v}_{i2}$ and $\vec{v}_{i3}$, see Fig. 3. The set $\Lambda_{hidden} \subset \Lambda$ are the points which belong to the infinite truncated tetrahedron whose base is the facet i and whose sides are determined by the vectors $\vec{v}_{i1}$, $\vec{v}_{i2}$ and $\vec{v}_{i3}$, see Fig. 3. The arbitrary point P is a member of Λ if its coordinates, α_1, α_2 and α_3, in the coordinate system formed by O, $\vec{v}_{i1}$, $\vec{v}_{i2}$ and $\vec{v}_{i3}$ are greater than zero[2]:

$$P \in \Lambda \leftrightarrow \overrightarrow{OP} = \alpha_1\vec{v}_{i1} + \alpha_2\vec{v}_{i2} + \alpha_3\vec{v}_{i3} \mid (\alpha_1 > 0) \wedge (\alpha_2 > 0) \wedge (\alpha_3 > 0) \tag{23}$$

The arbitrary point P is a member of the set Λ_{hidden} if it is a member of Λ and the sum of its coordinates, α_1, α_2 and α_3, in the coordinate system formed by O, $\vec{v}_{i1}$, $\vec{v}_{i2}$ and $\vec{v}_{i3}$ is greater than one:

$$P \in \Lambda_{hidden} \leftrightarrow \left(P \in \Lambda \wedge \sum_{i=1}^{3}\alpha_i > 1\right) \tag{24}$$

[Figure 3 about here.]

The latter condition can be easily understood when the equation of the plane of the facet in vector form is considered. A point P' is contained in the plane of the facet if:

$$\overrightarrow{OP'} = \vec{v}_{i1} + \lambda(\vec{v}_{i2} - \vec{v}_{i1}) + \mu(\vec{v}_{i3} - \vec{v}_{i1}) \quad \lambda \in \mathbb{R},\ \mu \in \mathbb{R}, \tag{25}$$

[2]Operator $\wedge$ means "and"

where $(\vec{v}_{i2} - \vec{v}_{i1})$ and $(\vec{v}_{i3} - \vec{v}_{i1})$ are a couple of vectors which determine the plane. Thus, the equation of the points of a parallel plane which is further from the radar P'' is:

$$\overrightarrow{OP''} = \kappa\vec{v}_{i1} + \lambda\left(\vec{v}_{i2} - \vec{v}_{i1}\right) + \mu\left(\vec{v}_{i3} - \vec{v}_{i1}\right) \quad \kappa > 1,\ \lambda \in \mathbb{R},\ \mu \in \mathbb{R}, \tag{26}$$

and the sum of its coordinates, κ, is greater than one, which agrees with (24). According to (24), if the coordinates of the barycenter of a facet j in the coordinate system formed by O, $\vec{v}_{i1}$, $\vec{v}_{i2}$ and $\vec{v}_{i3}$ are greater than zero and their sum is greater than one, the facet j is hidden by the facet i.

The algorithm starts finding the set of facets, Ψ, whose active face is facing the radar, i. e., the inner product of $\overrightarrow{OO_B}$ and $\hat{n}$ is less than zero. The facets whose active face is not facing the radar are always hidden so they are not taken into account in the next step of the algorithm so the computational burden is lowered. An illumination flag, whose initial value is one, is assigned to each facet of Ψ. The algorithm goes through Ψ, calculates the hidden facets per each facet of Ψ and sets their illumination flag to zero. At the end of the algorithm, the facets of Ψ whose illumination flag remains with value one are the visible ones and, therefore, ψ_i is determined.

III. Implementation considerations

This Section deals with the facet division algorithm, the SNR definition and the validation of our model as far as RCS computation of complex targets is concerned. The facet division algorithm is based on the Delaunay triangulation, which has been a technique widely used in different areas of study such as Mathematics, Computational Geometry, Topography and Electromagnetism [26], [27]. The validation of the model is carried out by calculating the radar cross section of several objects whose RCS was measured previously [19]. Our facet model shows an excellent agreement with the measurements when there is not multiple scattering.

A. Facet division algorithm

This Section deals with the development of a facet division algorithm based on Delaunay triangulation. The initial facets which compose the target are defined by the user. As these initial facets might be greater than the resolution cell and each facet only reflects in one resolution cell, a facet division algorithm is required so that the target reflects signal in all the resolution cells that it occupies. In addition, the accuracy of the shadowing algorithm improves when we increase the number of facets that model the target. Consequently, the aim of this subsection is to make the facets smaller than the range resolution cell.

The main property of the Delaunay triangulation is that it maximizes the minimum angle of all the angles of the triangles so the triangles tend to be more regular. Delaunay triangulation for a set P of points in the plane is a triangulation such that no point in P is inside the circumcircle of any triangle. In this paper, the initial set of points for each facet used to calculate the Delaunay triangulation is located on the three sides of the triangle. The distance between points d_i on the side i depends on the length of the side l_i, the range resolution ΔR and the user-defined parameter N:

$$d_i = \frac{l_i}{n_i} \tag{27}$$

$$n_i = \left\lceil \frac{N \cdot l_i}{\Delta R} \right\rceil \tag{28}$$

where $\lceil x \rceil$ stands for the ceiling function of x. From equations (27) and (28) it can be seen that the greater N is, the smaller the distance between points is and the smaller the resulting facets are. A higher value of N adds realism to the simulation concerning shadowing and cell migration effects. This algorithm is applied to all the facets of the target the number of times specified by the user. Various examples of the result of the algorithm are shown in this paper, Figs. 4, 6, 9 and 12.

B. Noise level considerations

It is desired to carry out simulations with the same noise level regardless of the target because the noise is mainly inherent to the receiver. It is assumed stationary complex white Gaussian noise (CWGN). The noise level and the received signal are defined without taking into account the noise factor, the antenna gain and the distance attenuation. As the noise level is the same regardless of the target, the user sets the SNR of the received signal, SNR_{ref}, considering a referential target whose radar cross section is 1 m^2 located in one resolution cell. In this case, the amplitude of the received signal is one according to equation (1). Therefore, the variance of the noise $n(t) = n_r(t) + j \cdot n_i(t)$, where the real and imaginary components are independent and identically distributed, is:

$$\sigma_r^2 = \sigma_i^2 = \left(2 \cdot 10^{\frac{SNR_{ref}}{10}}\right)^{-1} \tag{29}$$

where σ_r^2 and σ_i^2 are the variances of the real and imaginary part of the noise, and SNR_{ref} is expressed in dB, .

C. Validation of the model

The radar cross section of 3D objects can be computed with equation (1) when the whole object is in one resolution cell and there is no noise. This analysis is performed to validate our model although RCS calculation is not our main objective but the simulation of ISAR images of moving targets. The objects which have been chosen to calculate their radar cross sections are analyzed in [19]. The first object is a perfectly conducting sphere with radius 30.48 cm in front of a perfectly conducting plate whose dimensions are 50.8 cm height x 76.2 cm width x 2.54 cm depth, as illustrated in Fig. 4. The distance between these objects is 5.08 cm. The radar cross section for 10 GHz is shown in Fig. 5. The measured data are shown in Fig. 8 in [19]. In view of the measured data, the calculation of the RCS perfectly agrees with the measured RCS. The reason is that the multiple scattering is negligible in this case so the facet model is a good approximation.

[Figure 4 about here.]

[Figure 5 about here.]

The second object is an unconnected right-angle corner reflector, composed of two plates whose dimensions are 38.1 cm height x 30.48 cm width x 2.54 cm depth, separated 12.7 cm, as illustrated in Fig. 6. The radar cross section for 10 GHz is shown in Fig. 7. The measured data are shown in Fig. 9 in [19]. In view of the measured data, the calculation of the RCS does not agree with the measured data if the angle of incidence is approximately between -40º and 20º. This is due to the fact that the multiple scattering produces high RCS with these angles of incidence. When the angle of incidence is different from that interval, the agreement is excellent.

[Figure 6 about here.]

[Figure 7 about here.]

IV. ISAR IMAGES OF MOVING TARGETS

In this Section, we explain how to use our facet model in order to simulate ISAR images of moving targets. The diagram of the simulator is shown in Fig. 8. As the initial facets of the target could occupy several range cells, the first step is to calculate the target's facets that are actually used in the simulation by means of the algorithm proposed in subsection III-A. This algorithm, based on the Delaunay triangulation, makes use of the bandwidth of the signal to calculate the range resolution so that facets with appropriate size are generated. This bandwidth is assumed to be $B = 1/T$ where T is the duration of the transmitted pulse. As it is shown in Fig. 8, this triangulation step only takes place at the beginning of the simulation and the resulting facets are the ones that are actually used to compute the received signal. Then, according to the target's dynamics, the position of each facet is calculated at each transmitted pulse and the received signal from this pulse is obtained from equation (1). As the way of calculating the received signal at a time is independent of the target's dynamics, see Section II, our model is able to handle any kind of target's dynamics including rigid body motions or articulated motions. The received signal is sampled at B samples per second, i.e., there is one sample per range cell. Once these steps have been repeated for all the transmitted pulses, we obtain the range profiles and the ISAR image is formed by applying an FFT to the range profiles along the slow time [28]. In the following examples, motion compensation techniques are not used and a Hamming window is used to compute the FFT to lower the side-lobe effects.

[Figure 8 about here.]

First we analyze the ISAR image of a ship. The ship is following a straight line trajectory with a pitch rotational movement. The rotational movement of the ship is defined in the coordinate system $O'XYZ$ where O' is the geometric center of the target, the $O'X$ axis is located along the main axis of the ship, the $O'Y$ axis is located along the secondary axis and the $O'Z$ axis is orthogonal to the ground, see Fig. 9. The pitch rotation angle $\varphi(t)$, with respect to $O'Y$, is assumed to follow a sinusoidal variation:

$$\varphi(t) = \varphi_0 + A_\varphi \cos(2\pi f_R t) \tag{30}$$

where φ_0 is the initial angle, A_φ is the amplitude of the variation and f_R is the frequency of the movement. Accordingly, at each time step, the position of the ship regarding the linear motion is calculated and after that, it is rotated with respect to the $O'Y$ axis (pitch motion).

[Table 1 about here.]

The ship is moving away from the radar with a constant velocity following a straight line trajectory that forms 45º with respect to the line of sight as shown in Fig. 10. The simulation parameters are shown in Table I. The ship has 25985 facets and it takes 644 seconds to calculate the received signal for all the transmitted pulses using a 2.4 GHz processor. This computing time can be reduced by using more processors because our code is parallel, i. e., it is able to compute the received signal at a time without having calculated the received signal at previous times. This way, we can take advantage of the latest computers

that include several processors. The ISAR image of the ship is shown in Fig. 11. In general, an ISAR image is different from an optical image because it is motion dependent. Nevertheless, the shape of the ship in this ISAR image bears a strong resemblance with the optical image, i. e., we are able to identify the main features of the ship like the three masts, the hull and the bridge. This happens because a pitch motion in this scenario generates this kind of ISAR image in which the profile of the target is easily recognizable.

[Figure 9 about here.]

[Figure 10 about here.]

[Figure 11 about here.]

Now, we proceed to analyze the ISAR image produced by a Bo105 helicopter, shown in Fig. 12. As it is seen in this Figure, this sort of helicopter has a four-blade main rotor and a two-blade tail rotor. The parameters of the simulation are those in Table II. The helicopter has 7714 facets and it takes 190 seconds to calculate the received signal for all the transmitted pulses using a 2.4 GHz processor. The range profiles and the ISAR image of the helicopter are illustrated in Fig. 13 and 14, respectively. The range profiles are shown because it is easier to recognize the effects of the blades of the helicopter there than in the ISAR image. The periodic shapes that appear in the range profiles are due to the movement of the blades of the main rotor. In the ISAR image, we can see the body of the helicopter and two main vertical lines. Since the initial radial velocity of the helicopter is 1.82 m/s and it is flying away from the radar, the Doppler shift[3] is -109.2 Hz and, therefore, the body of the helicopter is placed around this frequency in Fig. 14. The most powerful vertical line, which is located on the right of the image, is caused by the echoes from the blades of the main rotor when their position is orthogonal to the line of sight and the vertical line on the left is caused also by the echoes from the blades of the main rotor when they are in their closest position to the radar. These vertical lines appear as the consequence of applying an FFT to a series of impulses of high power [20].

[Figure 12 about here.]

[Table 2 about here.]

[Figure 13 about here.]

[Figure 14 about here.]

V. Radar back-scattering from a human

In this Section, we describe the way to simulate the radar back-scattering from a human using computer animation data so as to show the capability of our simulator to deal with targets with nonrigid motions. Radar back-scattered signal from human gait has been recently studied [29], [30] because of its interesting applications in access control and surveillance. We model the human body by a set of ellipsoids composed by facets that move according to computer animation data recorded from real human's movement. The human gait is obtained using Acclaim's ASF/AMC files from [31]. These files were created by recording the position of several markers placed on a subject who was performing a certain action using twelve infrared cameras. Based on this acquisition, the files contain the movement information of the human "skeleton" made up of bones which connect certain joints [31]. Each animation is composed of two files, one with the extension ".asf" and another with the extension ".amc". In the former, the skeleton is defined at the beginning of the motion. In the latter, the motion data is given at the data acquisition rate of the cameras $f_a = 120$ Hz. Then, using the data in the ASF/AMC files and the Neil Lawrence's Motion Capture Toolbox [32], we obtain the positions of all the bones, described by the positions of their ends, when time t is $t = n_f/f_a$ where $n_f \in \{0,\ 1,\ ...,\ N_f - 1\}$ is the frame number and N_f is the number of frames captured by the cameras.

However, the positions of the bones must be known when the radar transmits a pulse, i. e., when $t = n_p/PRF$ where $n_p \in \{0,\ 1,\ ...,\ N_p - 1\}$ is the pulse number and N_p is the number of pulses transmitted by the radar. The positions of the ends of bone i recorded by the cameras are represented by the sequence of matrices $\mathbf{B}_i^f\,[n_f]$ of size 3×2 where the two columns represent the 3-D cartesian coordinates of each end. Similarly, the positions of the ends of the bone i when the radar transmits a pulse are represented by the sequence of matrices $\mathbf{B}_i^p\,[n_p]$. For simplicity, it is assumed that the PRF is multiple of f_a, $PRF = m \cdot f_a,\ m \in \mathbb{N}$, then $\mathbf{B}_i^p\,[n_p]$ is estimated by the lowpass linear interpolation[4] of $\mathbf{B}_i^f\,[n_f]$ with factor m described in [33].

In this paper, each bone of the skeleton is modeled by an ellipsoid composed of triangular facets. The length of each bone is fixed in the ASF/AMC format but, in our simulator, its thickness is user-defined and can be different from bone to bone on account of the fact that different parts of the body have a different size.

The block diagram of the software used to calculate the radar echoes is shown in Fig. 15. It is equivant to the diagram of the ISAR moving target simulator, see Fig. 8, with the differences that the human's dynamics are obtained from the ASF/AMC files and the facets of the human are calculated based on the ASF file and the user-defined ellipsoid widths. At the beginning

[3] $\left|f_{Doppler}\right| = \frac{2|\vec{v}_r|}{\lambda}$

[4] This interpolation is implemented in Matlab in the function "interp".

of the simulation, each ellipsoid is divided into facets and stored in memory. Then, at each transmitted pulse, as we know the location of the ends of each bone, contained in the matrices $\mathbf{B}_i^p[n_p]$, we can apply a geometrical transformation to locate each ellipsoid in its correct position and calculate the received signal with the procedure explained in Section II.

[Figure 15 about here.]

In this case study, we obtain the micro-Doppler signature of a human summing the complex range profiles along the range cells where the human is located and applying a time-frequency transform [30]. The carrier frequency of the transmitted signal is 20 GHz, PRF is 1200 Hz, the bandwidth is 150 MHz, and the person is walking away from the radar in the scenario shown in Fig. 16, in which the person is 30 meters far from the radar and the radar is placed at a 3-meter height. A motion sequence from the radar's point of view is shown in Fig. 17. The micro-Doppler signature is calculated by an STFT with a Hamming window of 128 samples and an overlap of 120 samples.

[Figure 16 about here.]

[Figure 17 about here.]

The micro-Doppler signature of a human walking is shown in Fig. 18. From the micro-Doppler signature of human gait, each forward leg swing appears as large peaks, and the left and right leg swings complete a gait cycle [29]. The micro-Doppler signature of two point-scatterers located on the left foot and on the left hand is shown in Fig. 19. Using this procedure that consists of placing point-scatterers in different parts of the body, we are able to identify the effect of different parts of the body on the micro-Doppler signature.

[Figure 18 about here.]

[Figure 19 about here.]

VI. Conclusions

We have proposed a model of target based on triangular facets, which is able to deal with moving targets that have nonrigid motions, so as to simulate ISAR images, radar back-scattering and radar cross sections. The computational burden is kept as low as possible by including an automatic facet division algorithm that depends on the bandwidth of the transmitted signal. Even though the model of the signal received from the target is simple because it does not deal directly with electromagnetic fields, it provides a great amount of information to analyze ISAR images and radar back-scattering in a lot of scenarios due to its ability to handle targets with nonrigid motions. Due to these interesting characteristics, this model can be used as a first step to develop tools to classify different kinds of targets by means of ISAR imaging or micro-Doppler signature. In the future, we will try to combine computer animation software, such as Autodesk® Maya®, with our facet model to carry out more realistic simulations of targets, especially, humans.

VII. Acknowledgments

This work was supported by Project TEC2008-02148 of the National Board of Scientific and Technological Research (CICYT).

Appendix

In this Appendix, we prove that the phase center tends to be the barycenter of the triangle when the angle of incidence tends to zero, $\theta \to 0$. Then, our aim is to compute the limit when $\theta \to 0$ in the equation (22):

$$x_{S_i}(\theta = 0) = \lim_{\theta \to 0} \frac{\angle \int_S e^{j2kx \sin\theta} dS}{2k \sin\theta} \tag{31}$$

where $x_{S_i}(\theta = 0)$ is the location of the phase center when $\theta = 0$ and we denote $x = x_{SR}$ to employ a clearer notation. The limit in equation (31) can be also expressed as:

$$x_{S_i}(\theta = 0) = \lim_{\theta \to 0} \frac{\angle \int_S [\cos(2kx \sin\theta) + j \sin(2kx \sin\theta)] dS}{2k \sin\theta} =$$

$$= \lim_{\theta \to 0} \frac{\angle \left[\int_S \cos(2kx \sin\theta) dS + j \int_S \sin(2kx \sin\theta) dS\right]}{2k \sin\theta} \tag{32}$$

Taking into account that $\int_S \cos(2kx \sin\theta) dS$ and $\int_S \sin(2kx \sin\theta) dS$ are real numbers because the integrals only involve real numbers, equation (32) can be expressed as:

$$x_{S_i}(\theta = 0) = \lim_{\theta \to 0} \frac{\arctan \frac{\int_S \sin(2kx \sin\theta) dS}{\int_S \cos(2kx \sin\theta) dS}}{2k \sin\theta} \tag{33}$$

When $\theta \to 0$ in equation (33), the numerator and the denominator tend to zero so we apply the l'Hôpital's rule to solve the uncertainty calculating the derivatives of the numerator and denominator:

$$x_{S_i}(\theta = 0) = \lim_{\theta \to 0} \frac{\left[\frac{\int_S \sin(2kx\sin\theta)dS}{\int_S \cos(2kx\sin\theta)dS}\right]' \frac{1}{1+\left[\frac{\int_S \sin(2kx\sin\theta)dS}{\int_S \cos(2kx\sin\theta)dS}\right]^2}}{2k\cos\theta} \tag{34}$$

where the superscript ' denotes derivative. Continuing the procedure:

$$x_{S_i}(\theta = 0) =$$

$$= \lim_{\theta \to 0} \frac{\frac{\int_S 2kx\cos\theta\cos(2kx\sin\theta)dS \int_S \cos(2kx\sin\theta)dS - \int_S \sin(2kx\sin\theta)dS \int_S (-1)2kx\cos\theta\sin(2kx\sin\theta)dS}{\left[\int_S \cos(2kx\sin\theta)dS\right]^2} \frac{1}{1+\left[\frac{\int_S \sin(2kx\sin\theta)dS}{\int_S \cos(2kx\sin\theta)dS}\right]^2}}{2k\cos\theta} \tag{35}$$

In equation (35), the limit is easily calculated as there is no indetermination:

$$x_{S_i}(\theta = 0) = \frac{\int_S 2kxdS \int_S dS}{2k\left[\int_S dS\right]^2} = \frac{\int_S 2kxdS \cdot A_S}{2k\left[A_S\right]^2} = \frac{\int_S xdS}{A_S} \tag{36}$$

The term $\frac{\int_S xdS}{A_S}$ is the x coordinate of the barycenter of the facet by definition [34]. Therefore, as we have placed the barycenter in the origin of the coordinate system O_BXYZ_{SR}, $x_{S_i}(\theta = 0) = 0$. As the phase center has coordinates $(x_{S_i}, 0, 0)$ in the coordinate system O_BXYZ_{SR}, when $\theta = 0$, the phase center is the barycenter of the triangle.

REFERENCES

[1] V. C. Chen and W. J. Miceli, "Simulation of ISAR imaging of moving targets," in *IEE Proceedings Radar, Sonar and Navigation*, Volume 148, Issue 3, pp. 160-166, June 2001.

[2] A. Ausherman, A. Kozma, J. L. Waker, J, H. M. Jones, and E. C. Poggio, "Development in radar imaging," in *IEEE Transactions on Aerospace and Electronic Systems*, Volume 20, pp. 363-400, 1984.

[3] C. C. Chen, H. C. Andrews, "Target motion induced radar imaging," in *IEEE Transactions on Aerospace and Electronic Systems*, Volume 16, pp. 2-14, 1980.

[4] Zhishun She, Zhaoda Zhu, "Motion compensation of ISAR in frequency domain," in *Proceedings of the IEEE 1993 National Aerospace and Electronics Conference*, NAECON 1993 , Volume 1, pp. 299-302, 1993.

[5] D. Yau, P. E. Berry, B. Haywood, "Eigenspace-based motion compensation for ISAR target imaging," in *EURASIP Journal on Applied Signal Processing*, Volume 2006, Issue 1, pp. 134-134, 2006.

[6] A. Jain, I. Patel, "SAR/ISAR imaging of a nonuniformly rotating target," in *IEEE Transactions on Aerospace and Electronic Systems*, Volume 28, Issue 1, pp. 317-321, January 1992.

[7] T. Itoh, H. Sueda, Y. Watanabe, "Motion compensation for ISAR via centroid tracking," in *IEEE Transactions on Aerospace and Electronic Systems*, Volume 32, Issue 3, pp. 1191 - 1197, July 1996.

[8] J. M. Muñoz-Ferreras, F. Perez-Martínez, "Non-uniform rotation rate estimation for ISAR in case of slant range migration induced by angular motion," in *IET Radar, Sonar and Navigation*, Volume1, Issue 1, pp. 251 - 260, August 2007.

[9] O. A. Yeste-Ojeda, J. Grajal, "Atomic decomposition for ISAR imaging," in *IEEE Conference on Radar 2006* , pp. 504-509, April 2006.

[10] V. C. Chen, S. Qian, "Time-frequency transform vs. Fourier transform for radar imaging," in *Proceedings of the IEEE-SP International Symposium on Time-frequency and Time-scale analysis*, pp. 389 - 392, June 1996.

[11] V. C. Chen, W. J. Miceli, "Time-varying spectral analysis for radar imaging of manoeuvring targets," in *IEE Proceedings Radar, Sonar, Navigation*, Vol 145, No.5, pp. 262 - 268, October 1998.

[12] A. D. Lanterman, D. C. Munson, Jr. and Y. Wu, "Wide-angle radar imaging using time-frequency distributions," in *IEE Proceedings Radar Sonar Navigation*, Vol. 150, No. 4, pp. 203-211, August 2003.

[13] T. Thayaparan, G. Lampropoulos, S. K. Wong and E. Riseborough, "Application of adaptive joint time-frequency algorithm for focusing distorted ISAR images from simulated and measured radar data," in *IEE Proceedings Radar Sonar Navigation*, Vol. 150, No. 4, pp. 213-220, August 2003.

[14] G. López-Risueño, J. Grajal and O. Yeste-Ojeda, "Atomic decomposition-based radar complex signal interception," in *IEE Proceedings Radar Sonar Navigation*, Vol. 150, No. 4, pp. 323-331, August 2003.

[15] V. C. Chen, "Time-frequency based radar image formation," in *International Conference on Image Processing, 2004. ICIP '04*, Volume 1, pp. 1-4, October 2004.

[16] V. C. Chen and H. Ling, *Time-frequency transforms for radar imaging and signal analysis*, Artech House, 2002.

[17] I. S. Choi, B. L. Cho and H. T. Kim, "ISAR motion compensation using evolutionary adaptive wavelet transform," in *IEE Proceedings Radar Sonar Navigation*, Vol. 150, No. 4, pp. 229-233, August 2003.

[18] V. C. Chen and C. Lin and W. P. Pala, "Time-Varying Doppler Analysis of Electromagnetic Backscattering From Rotating Object," in *IEEE Conference on Radar 2006* , pp. 807-812, 2006.

[19] N. N. Youssef, "Radar cross section of complex targets," in *Proceedings of the IEEE*, Volume 77, Issue 5, pp. 722 - 734, May 1989.

[20] A. F. García-Fernández, J. Grajal, O. A. Yeste-Ojeda, "Analysis of ISAR images of a helicopter by a facet model," *Proceedings of the 2008 International Conference on Radar,* Adelaide, pp. 32-37, September 2-5, 2008.

[21] M. F. Catedra, J. Perez, "Application of physical optics to the rcs computation of bodies modeled with nurbs surfaces," in *IEEE Transactions on Antennas and Propagation*, Volume 42, Issue 10, pp. 1404-1411, October 1994.

[22] A. Boag, "A fast physical optics (FPO) algorithm for high frequency scattering," in *IEEE Transactions on Antennas and Propagation*, Volume 52, Issue 1, pp. 197- 204, January 2004.

[23] B. van den Broek, T. Bieker, L. van Ewijk, "Comparison of Modelled to Measured High-Resolution ISAR data," *TNO Defense, Security and Safety*, The Hague, The Netherlands, 2005.

[24] Wen Xiaoyang; Wang Chao; Zhang Hong, "Complex object's ISAR image simulation," *Geoscience and Remote Sensing Symposium*, 2005. IGARSS '05. *Proceedings*. 2005 IEEE International , vol.5, no., pp. 3181-3183, 25-29 July 2005.
[25] D. E. Kerr, *Propagation of short radio waves*, McGraw - Hill, 1951.
[26] L. F. Garcia, O. A. Mohammed, "Automatic finite element grid generation in electromagnetics," in *IEEE Conference Proceedings Southeastcon* '88, pp. 571 - 575 , April 1988.
[27] Zhou Jian-Ming; Shao Ke-Ran; Zhou Ke-Ding; Zhan Qiong-Hua, "Computing constrained triangulation and Delaunay triangulation: a new algorithm," in *IEEE Transactions on Magnetics*, Volume 26, Issue 2, pp. 694 - 697. March 1990.
[28] D. R. Wehner, *High-Resolution Radar*, Artech House, 1995.
[29] V. C. Chen, F. Li, S. Ho, H. Wechsler "Micro-Doppler effect in radar: phenomenon, model, and simulation study," *in IEEE Transactions on Aerospace and Electronic Systems*, vol.42, no.1, pp. 2-21, Jan. 2006.
[30] Victor C. Chen, "Detection and analysis of human motion by radar," *Proceedings of the 2008 IEEE Radar Conference,* Rome, pp. 1957-1960, May 26-30, 2008.
[31] Website of the Motion Research Laboratory, Carnegie Mellon University: http://mocap.cs.cmu.edu.
[32] N. D. Lawrence, "Mocap toolbox for MATLAB". Available on-line: http://www.cs.man.ac.uk/~neill/mocap
[33] *Programs for Digital Signal Processing*, IEEE Press, New York, 1979, Algorithm 8.1.
[34] M. Alonso, E. J. Finn, *Fundamental University Physics, Volume I Mechanics*, Addison-Wesley Publishing Company, Reading, Massachusetts, 1967.

Ángel F. García-Fernández received his degree in Telecommunication Engineering (with honours) from Universidad Politécnica de Madrid in 2007. Since 2007 he has been working towards the Ph.D. degree at the Department of Signals, Systems and Radiocommunications of the same University. His research activities and interests are in the area of target tracking using particle filters, wireless sensor networks, and radar signal processing.

Omar A. Yeste-Ojeda was born in Sta. Lucía de Tirajana (Las Palmas), Spain, in 1979. He received the Ingeniero de Telecomunicación degree and the Ph.D. degree from the Technical University of Madrid, Madrid, Spain in 2002 and 2007, respectively. Since then, he has been Research Assistant at the Signals, Systems, and Radiocommunications Department of the same University, where he is currently Associate Professor. His research activities are in the area of signal processing, with special focus on cyclostationarity and time-frequency analysis for signal interception and identification.

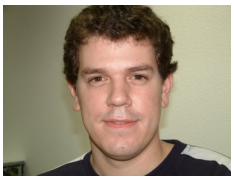

Jesús Grajal was born in Toral de los Guzmanes (León), Spain, in 1967. He received the Ingeniero de Telecomunicación and the Ph.D. degrees from the Technical University of Madrid, Madrid, Spain in 1992 and 1998, respectively. Since 2001 he has been an Associate Professor at the Signals, Systems, and Radiocommunications Department of the Technical School of Telecommunication Engineering of the same University. His research activities are in the area of hardware-design for radar systems, radar signal processing and broadband digital receivers for radar and spectrum surveillance applications.

LIST OF FIGURES

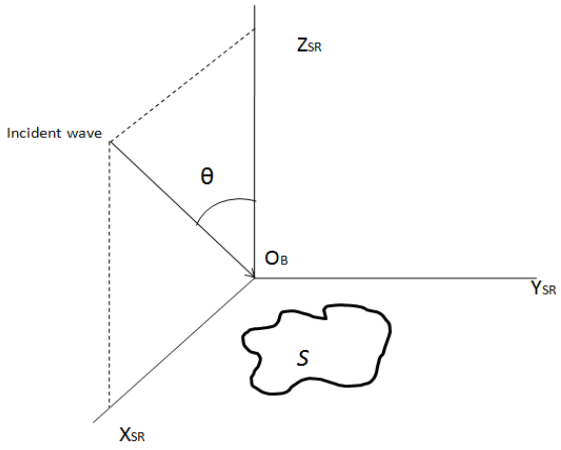

Figure 1: Geometry of the radar cross section calculation of a plane surface

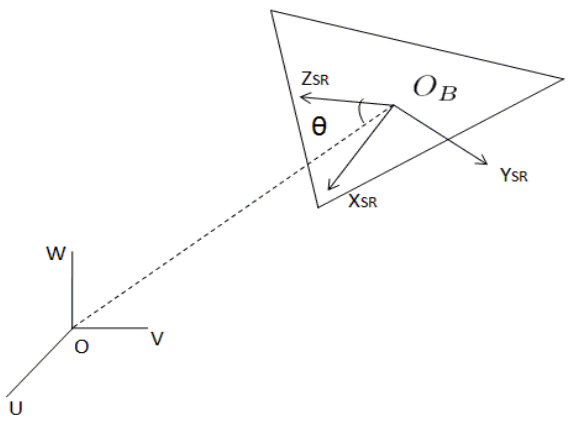

Figure 2: Geometry of the radar cross section calculation of a facet

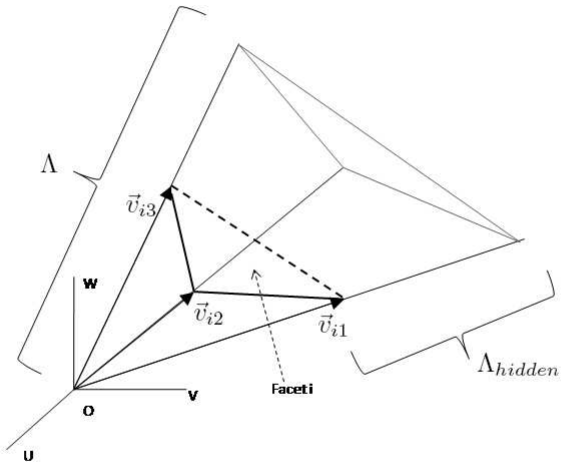

Figure 3: Geometry of hidden facets

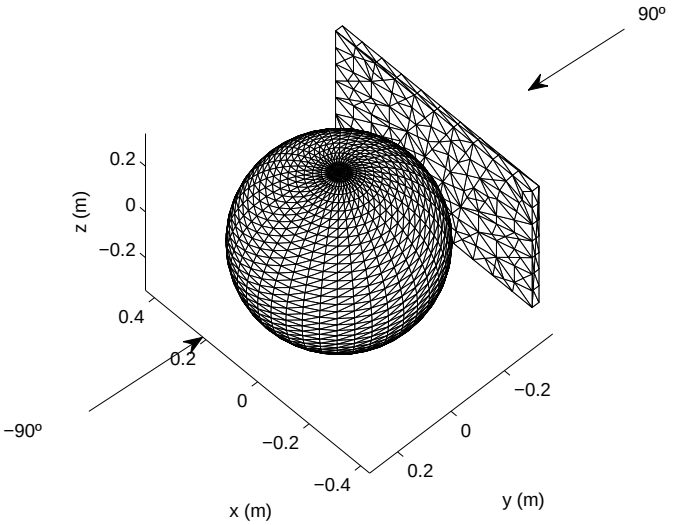

Figure 4: Sphere and vertical flat plane

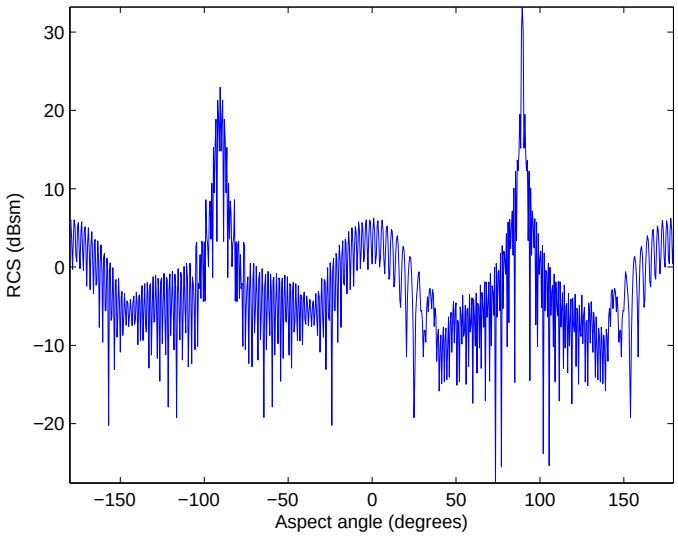

Figure 5: Calculated RCS for sphere and vertical flat plate, illustrated in Fig. 4 (measurements in Fig. 8 in [19])

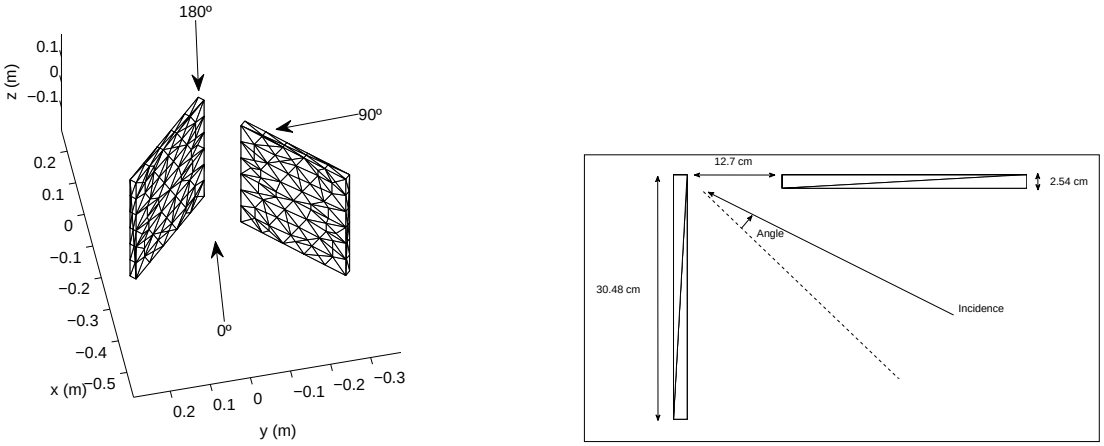

(a) 3D geometry

(b) Unconnected facets from above

Figure 6: Unconnected facets

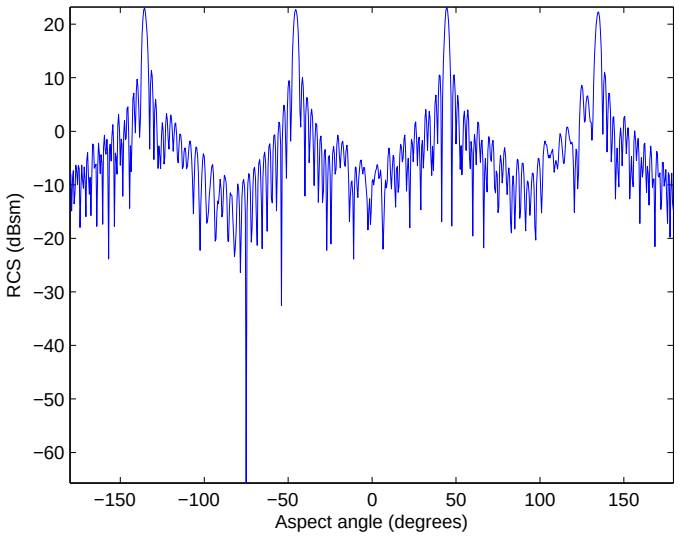

Figure 7: Calculated RCS for unconnected facets, illustrated in Fig. 6 (measurements in Fig. 9 in [19])

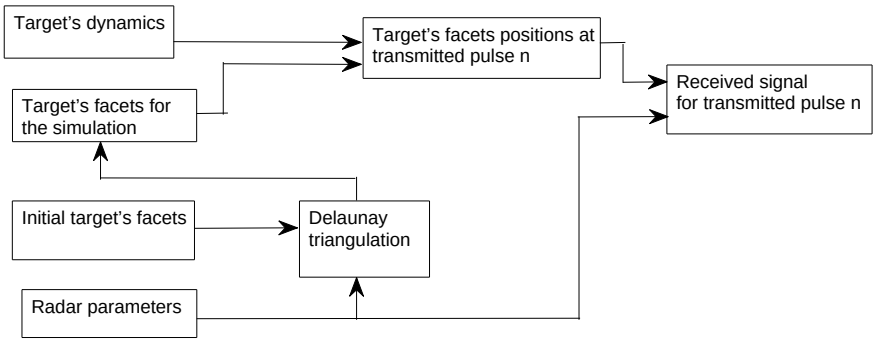

Figure 8: Diagram of ISAR moving target simulator

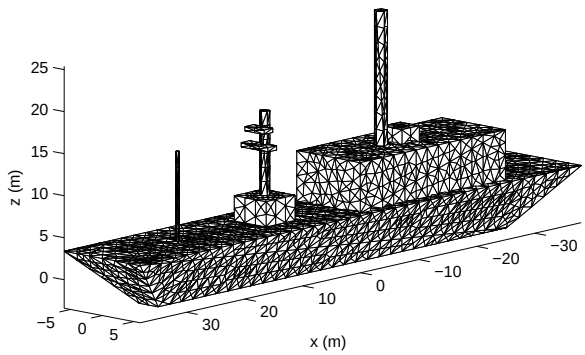

Figure 9: Facet model of the ship

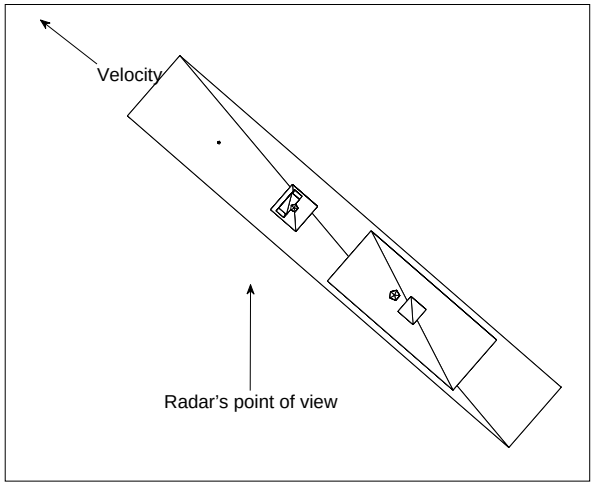

Figure 10: Trajectory of the ship

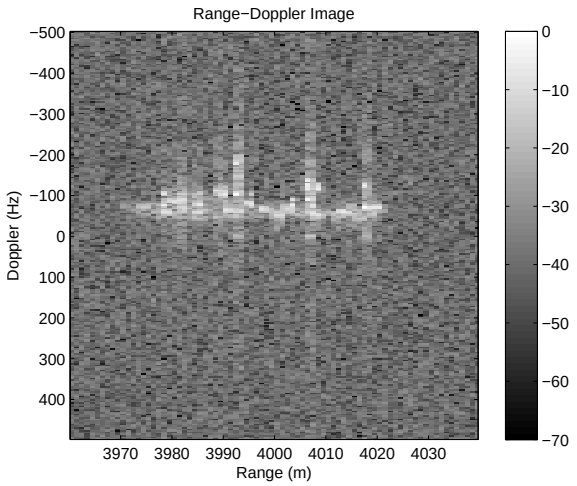

Figure 11: ISAR image of the ship

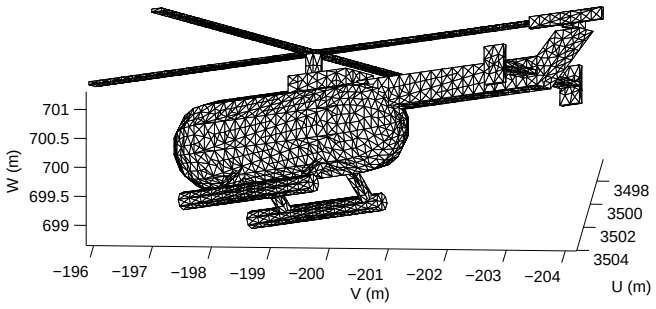

Figure 12: Optical image of the helicopter from the radar's position

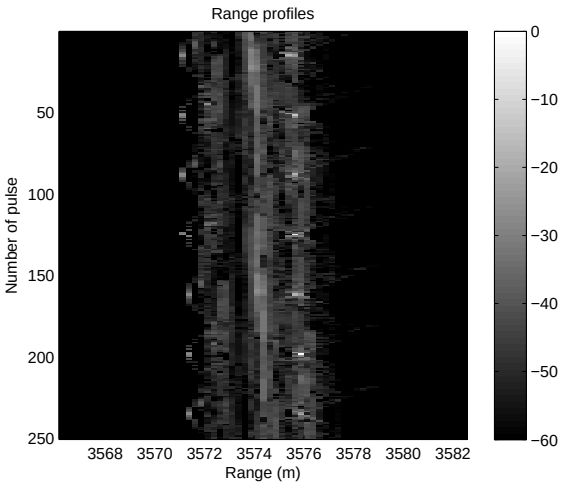

Figure 13: Range profiles of the helicopter

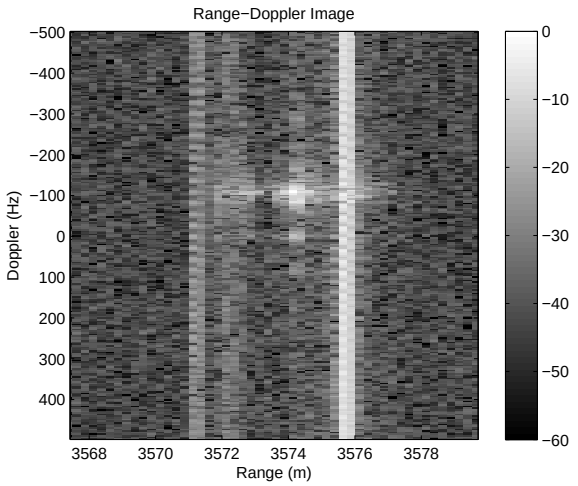

Figure 14: ISAR image of the helicopter

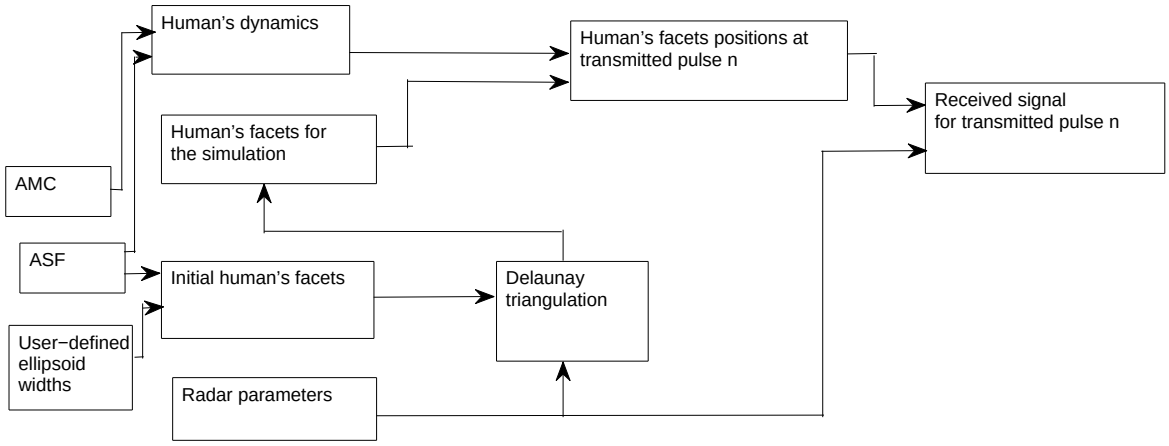

Figure 15: Diagram of the simulator of radar echoes from humans

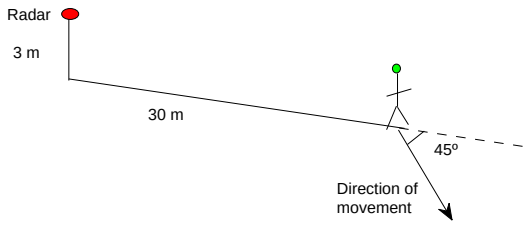

Figure 16: Case study scenario

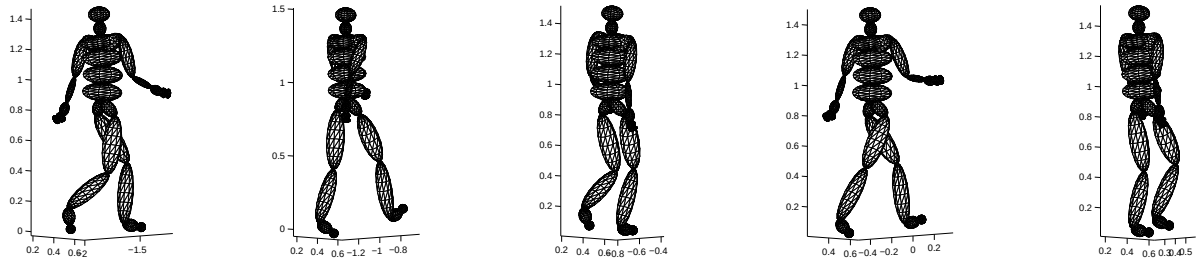

(a) 0.3s (b) 0.6s (c) 0.9s (d) 1.2s (e) 1.5s

Figure 17: Motion sequence

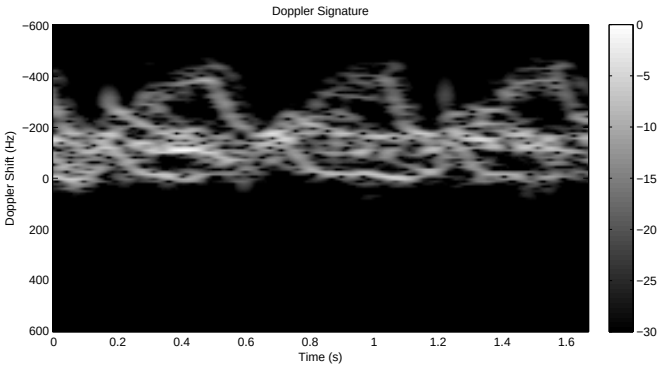

Figure 18: Doppler signature of the human walking

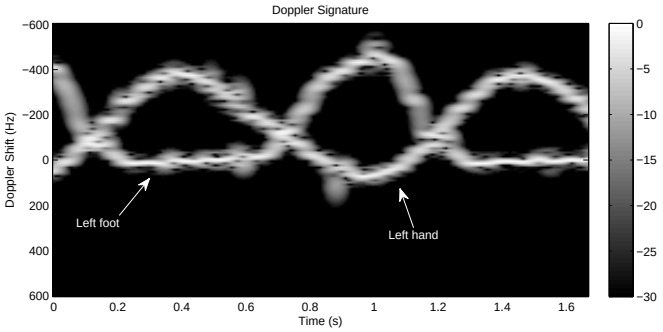

Figure 19: Left hand and left foot Doppler signature

List of Tables

Trajectory	Straight line
Initial coordinates (m)	(U, V, W) = (4000, 0, 0)
Velocity vector(m/s)	(v_U, v_V, v_W) = (1, 1, 0)
Kind of rotation	Sinusoidal Pitch
Amplitude A_φ	5@ @$_x$101012.0pt3.14996pt plus 4.49998pt1/ptm/m/n/10 @update @update o
Initial angle φ_0	0@ @$_x$101012.0pt3.14996pt plus 4.49998pt1/ptm/m/n/10 @update @update o
Rotation frequency f_R	1/5 Hz
Carrier frequency	9 GHz
Bandwidth	150 MHz
PRF	1 kHz
Number of pulses	250
SNR$_{ref}$	25 dB
Facet division algorithm parameters	$N = 1.1$ Four iterations

Table I: Simulation parameters for the ship

Trajectory	Straight line
Initial coordinates (m)	$(U,\, V,\, W)$ = $(3500,\, -200,\, 700)$
Velocity vector(m/s)	$(v_U,\, v_V,\, v_W)$ = $(2,\, 2.5,\, 0)$
Blades rotation rate (@ $^{@_x}$101012.0pt3.14996pt plus 4.49998pt1/ptm/m/n/10 @update @update $^{\circ}/\mathrm{s}$)	2463.7
Tip speed of main rotor blades (m/s)	215
Carrier frequency	9 GHz
Bandwidth	600 MHz
PRF	1 kHz
Number of pulses	250
SNR_{ref}	35 dB
Facet division algorithm parameters	$N = 1.1$ Four iterations

Table II: Simulation parameters for the helicopter